Tractometric Coherence of Fiber Bundles in DTI

Rick Sengers[1(✉)], Tom Dela Haije[2], Andrea Fuster[1], and Luc Florack[1]

[1] Eindhoven University of Technology, Eindhoven, The Netherlands
{H.J.C.E.Sengers,A.Fuster,L.M.J.Florack}@tue.nl
[2] University of Copenhagen, Copenhagen, Denmark
tom@di.ku.dk

Abstract. Based on a diffusion tensor image (DTI) and a tentative tractogram of a fiber bundle we propose a filtering method for operationally defining and removing outliers using tractometry. To this end we assign to each track a set of K invariants, i.e. scalars invariant under rigid transformations. The cluster of K-tuples of all tracks in a bundle may be pruned using outlier detection methods in $\mathbb{R}^K$, after which back-projection of the remaining K-tuples produces a filtered tractogram with enhanced coherence. This intrinsic pruning method is blind to the relative spatial organization of tracks in a bundle. We consider two types of invariants, one capturing local diffusion properties and one representing differential properties averaged along tracks. Our experiments indicate that our tractometric filtering is complementary to extrinsic methods based on the relative spatial configuration of tracks.

Keywords: Diffusion tensor imaging · Tractography · Tractometry · Tractography filtering · Riemannian geometry

1 Introduction

Tractography aims at reconstructing fiber bundles in the brain from diffusion weighted imaging (DWI), a non-invasive technique for in-vivo imaging of the brain's fibrous structure. For our purpose tractography may refer to any method providing a bundle of tentative tracks, the most prevalent being either streamline methods based on diffusion tensor imaging (DTI) [2,4,28,37], or geodesic methods [11,15,16,20,25,28,30], whether deterministic or probabilistic.

Given two regions of interest (ROI) any of these methods may yield a collection of putative tracts in-between. In streamline methods this is achieved by designating one ROI as the seed region from which tracks are initialised to define integral curves of some a priori preferred diffusion direction, e.g. the main eigendirection of the diffusion tensor in the case of deterministic tractography based on DTI. In this case the second ROI serves as an include-region which ensures only tracks that pass through it are kept in the tractogram. In geodesic tractography tracks are curves of (locally) shortest length in a Riemannian (or more generally, Finslerian) space, i.e. geodesics [1,17,27,29,32]. The associated

S. Cetin-Karayumak et al. (Eds.): CDMRI 2022, LNCS 13722, pp. 137–148, 2022.
https://doi.org/10.1007/978-3-031-21206-2_12

metric is constructed on the basis of the DTI (or DWI) data in such a way that small distances in Riemannian (or Finslerian) sense are tantamount to large mean free paths. In this case both ROIs are necessary for disambiguation due to the second order nature of geodesic tractography. Geodesic completeness (aka the Hopf-Rinow Theorem) ensures that at least one connection between any two given endpoints exists.

In all cases we obtain as a starting point a single-bundle tractogram consisting of, say, N tracks. This tractogram may contain 'incoherent' fibers, i.e. outliers (not necessarily false positives) that significantly deviate from the main bundle in one way or another. Our goal is to obtain a filtered tractogram of $M \leq N$ selected tracks that, in some precise sense, exhibit more coherence. Instead of utilizing solely spatial information, e.g. as in [13,14,19,22,26] or streamline densities [33] or the diffusion signal [10], we aim to do this by means of *tractometry*, the assignment of characteristic scalars to each track. Tractometry has been used for various purposes, such as dimensionality reduction [7], tract-analysis [38] and anomaly detection [6]. Tractometric scalars can also be used to prune a tractogram by eliminating $N-M$ tracks (with M an automatic or manual control parameter) that are deemed deviatory according to some coherence measure. Underlying this is the assumption that microstructural similarities within a particular anatomical (sub)bundle are reflected in a (macroscopic) similarity among the assigned scalars for that (sub)bundle, i.e. assuming no counteracting pathological effects [6,35]. For this reason we stress that we do not consider the method to work globally on a whole brain tractogram, but as a a single-bundle method pruning its streamlines one by one.

2 Theory

In principle any ad hoc set of scalar functionals could be used in the proposed tractometry framework. However, we will formulate a set of criteria, the first of which pertains to *invariance* under rotations. If f is a scalar function of a diffusion tensor D, it is invariant under rotations if $f(D) = f(R^T DR)$ for any rotation matrix R. We will refer to such invariant scalar functions simply as 'invariants'. An example of a non-invariant scalar would be any isolated component of the diffusion tensor D, whereas the trace $\mathrm{Tr}(D)$ *is* an invariant. Global, track-wise invariants may be constructed from point-wise invariants sampled along a track by taking their average, median, minimum, maximum, or other integral measures. In the rest of the paper we will use the mean for the sake of definiteness.

Secondly, we require an admissible set of invariants to satisfy well-defined *non-redundancy* and *completeness* conditions. These conditions capture the notion of the set containing 'precisely enough' information.

Let V be the space of all possible invariants and $W \subset V$ a subset. A set $X = \{x_1, ..., x_n\} \subset V$ is said to be redundant if there exists an analytic function f such that $x_n = f(x_1, ..., x_{n-1})$. Equivalently, X is non-redundant if

$$f(x_1, ..., x_n) = 0 \quad \Longrightarrow \quad f \equiv 0\,. \tag{1}$$

The set X is complete in W if it generates W with analytic functions, i.e. W is the image of X under analytic functions

$$\{x \in V \mid x = f(x_1, ..., x_n) \text{ for some analytic } f\} = W\,. \tag{2}$$

Consider the set

$$\{t_k \doteq \mathrm{Tr}(D^k), t_{k+1} \doteq \mathrm{Tr}(D^{k+1}), t_{k+2} \doteq \mathrm{Tr}(D^{k+2})\} \tag{3}$$

of Euclidean traces of powers of the diffusion tensor D. For any $k \in \mathbb{N}$ this set is a complete and non-redundant set of invariants by virtue of the Cayley-Hamilton theorem. The example simultaneously illustrates the non-uniqueness property of a tractometric framework. We may arbitrarily choose traces of any three consecutive powers of D to construct a non-redundant complete invariant set. Alternatively we may replace such trace-triples by eigenvalue-triples $\{\lambda_1, \lambda_2, \lambda_3\}$ of D, or by their combinations $\{\mathrm{FA}, \mathrm{MD}, \mathrm{RD}\}$, known as the fractional anisotropy, mean diffusivity and radial diffusivity [3]. These invariants will be refered to as *diffusion invariants*, since they explicitly relate to apparent diffusion properties.

Besides diffusion invariants we wish to include differential properties, taking into account local information in the neighbourhood of a track, i.e. *geometry*. We will make use of the so-called *curvature invariants*, constructed from the Riemann curvature tensor. This tensor determines geodesic deviation [1,31,32,34], and in the context of geodesic tractography it expresses the tendency of nearby tracks to cohere or repel due to local inhomogeneities in the diffusion tensor field. In our Riemannian approach the diffusion tensor D, with components D^{ij} $(i, j = 1, 2, 3)$ relative to a Cartesian coordinate basis, is stipulated to be proportional to the dual Riemannian metric g^{-1}, with components[1] g^{ij}, i.e. $D^{ij} \propto g^{ij}$, so as to 'geometrize away' local diffusivity patterns in the data [11,16,20,25]. Anisotropic water diffusion is then incorporated as intrinsic geometry representing isotropic diffusion in a curved, Riemannian space.

The Riemann curvature tensor R^i_{jkl} is constructed from second order derivatives of the metric tensor, as follows :

$$R^i_{jkl} = \partial_k \Gamma^i_{jl} - \partial_l \Gamma^i_{jk} + \Gamma^i_{km}\Gamma^m_{jl} - \Gamma^i_{lm}\Gamma^m_{jk}\,, \tag{4}$$

where

$$\Gamma^i_{jk} = \frac{1}{2} g^{im} \left(\partial_j g_{km} + \partial_k g_{mj} - \partial_m g_{jk}\right)\,, \tag{5}$$

and in which ∂_k stands for $\partial/\partial x^k$. Contraction of the Riemann tensor results in the covariant Ricci curvature tensor as well as its mixed and contravariant forms by raising indices with the help of the inverse metric tensor:

$$R_{ij} = R^k_{ikj} \quad R^i_j = g^{ik} R_{kj} \quad \text{and} \quad R^{ij} = g^{ik} g^{jl} R_{kl}\,. \tag{6}$$

[1] Super-/subscripts denote contra-/covariant indices, to which Einstein summation convention applies, i.e. each pair of identical sub- and superscript implies a summation over the corresponding 'dummy' index.

In turn, the Ricci tensor induces a set of curvature invariants given by

$$\{r_1 \doteq R^i_i, r_2 \doteq R^i_j R^j_i, r_3 \doteq R^i_j R^j_k R^k_i\}\,, \tag{7}$$

in which r_1 is known as the Ricci scalar [8,9]. Thus the set $\{r_1, r_2, r_3\}$ is composed of traces of powers of the matrix with entries R^i_j. By similar arguments as for the diffusion invariants we may instead consider the set $\{\mu_1, \mu_2, \mu_3\}$ of eigenvalues of this matrix.

In either case we prefer the use of eigenvalues $\{\lambda_1, \lambda_2, \lambda_3\}$ and $\{\mu_1, \mu_2, \mu_3\}$ over traces $\{t_1, t_2, t_3\}$, respectively $\{r_1, r_2, r_3\}$, because the former are commensurable and of the same order of magnitude, unlike the latter. Diffusion and curvature invariants provide two complete, non-redundant sets of three invariants each, which we can use separately or jointly as our tractometric invariants of choice.

Given a tractogram of a putative bundle between two anatomical ROIs, we wish to prune it based on the above sets of diffusion and/or curvature invariants by removing 'incoherent' tracks one-by-one in some hierarchical fashion. Consider a bundle of N tracks, each with K associated (averaged) invariants. We thus obtain a correspondence between tracks and points in $\mathbb{R}^K$, yielding a point cloud for the bundle of interest. This point cloud is subsequently pruned with the help of an outlier detection method [5,18,21]. We found that the particular choice of outlier detection method had little effect on the outcome, and chose to use the *isolation forest* algorithm [21]. This algorithm assigns to each cloud point an 'incoherence' score between 0 and 1, indicating its likeliness to be an anomaly within the considered set. A score of 0.5 is then a natural threshold for a particular sample to be labelled as either outlier (score > 0.5) or not (score ≤ 0.5). This threshold could subserve a baseline configuration from which to initialise further pruning by more informed means, possibly involving human interaction. The incoherence score imposes a ranking onto tracks, allowing them to be hierarchically removed one-by-one, cf. Fig. 1.

3 Experiments

In the following experiments we illustrate the tractometric filtering framework on a DWI dataset from the Human Connectome Data Project (dataset "WU-Minn HCP Data-1200 Subjects": subject 100307; TE/TR/echo spacing 89.5/5520.0/0.78 ms; b = 2000 s/mm^2), as well as on a clinical dataset acquired with a Philips Achieva 3T MRI scanner (b = 1500 s/mm^2, 50 diffusion-weighting directions, six b = 0 s/mm^2 images, 2 mm isotropic voxel size, TE/TR/echo spacing 87/8000/0.2 ms). DTI tensors are computed using weighted least squares via the Dipy library in Python [12]. Throughout our experiments the defining Gram matrix for the Riemannian metric is the adjugate of the diffusion tensor D, i.e. $g_{ij} = \det(D) D^{\text{inv}}_{ij}$, cf. Fuster et al. [11].

We consider two experiments, the corticospinal tract (CST) on the HCP dataset and the arcuate fasciculus (AF) on the clinical dataset, to illustrate that the proposed method has a qualitatively different behaviour on a per bundle

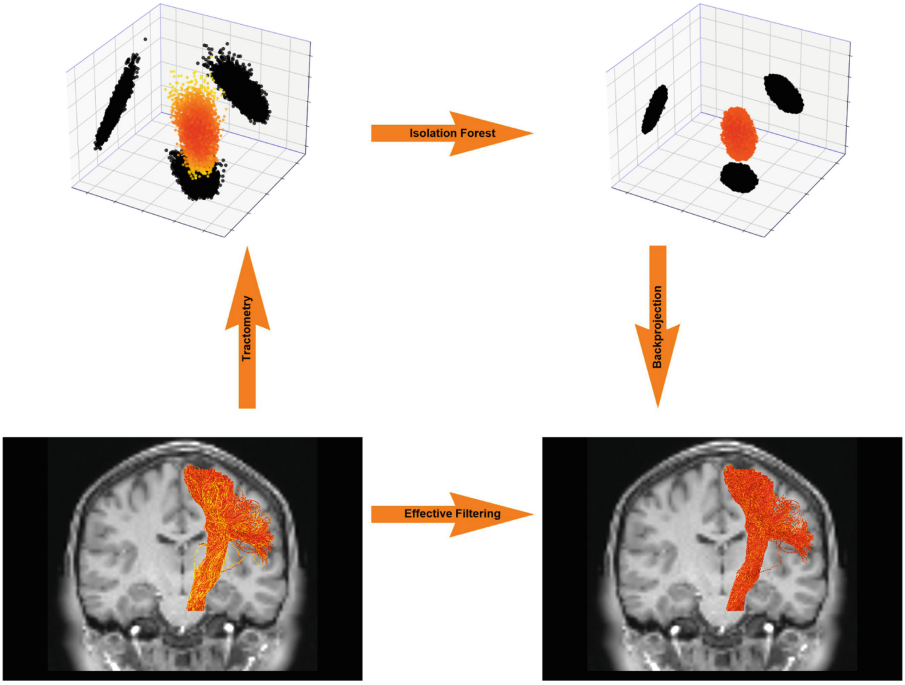

Fig. 1. An example of the filtering method for the corticospinal tract (CST) using the diffusion invariants. **Top left:** Scatterplot of the three invariants $\{\lambda_1, \lambda_2, \lambda_3\}$ for each of the 7500 tracks in the tractogram, color-coded according to the isolation score as determined by the isolation forest algorithm. Each invariant $\{\lambda_1, \lambda_2, \lambda_3\}$ is projected onto the coordinate planes in black. **Top right:** Scatterplot of the invariants after removing all points with isolation score larger than 0.5. **Bottom:** Tractograms corresponding to the scatterplots above, with the unfiltered tractogram on the left and the filtered one on the right. The arrow 'Effective Filtering' is defined by virtue of the other three, 'Tractometry', 'Isolation Forest' and 'Backprojection'.

basis. Furthermore, these two bundles are of clinical interest to a collaborating neurosurgeon, clarifying the use of a clinical dataset in the AF-experiment. Both experiments are set up according to the following structure. We depart from a probabilistic streamline tractogram computed using the iFOD2 algorithm included in *tckgen* in MRtrix3 [36] following the data processing pipeline described in [23]. We then apply four different filterings, three of which are based on our tractometric invariants, viz. the set of three diffusion invariants, the set of three curvature invariants, respectively and their union (containing all six invariants). All track-wise invariants are computed by sampling the voxel-wise invariants along the curve using trilinear interpolation. The fourth filtering, introduced as comparison reference, relies on a scalar measure based on the relative spatial arrangement of tracks in a bundle, the Fiber-to-Bundle Coherence (FBC) [22]. This provides us with a comparison between our tractometric

filtering based on intrinsic invariant features of each track regardless of spatial coherence, and one based on relative spatial relations between tracks, but blind to their intrinsic features. Figure 2 shows the baseline tractogram with the corresponding diffusion and curvature invariants for the experiments on the CST and the AF.

Figure 3 illustrates the filtering procedures applied to the CST tractogram using the HCP dataset. Since the FBC score and the isolation score are incommensurable we opt to retain a fixed number of tracks in every step, instead of thresholding on the scores themselves. We start with 7500 tracks and retain 50% in the first step and 10% in the last one. The used colormaps are such that bright-colored tracks correspond to outliers in the scatterplots, and vice versa for dark-colored tracks. All tracks in the 90% filtered tractograms are also present in the 50% filtered one, but are mostly obscured by other tracks. The three tractometric filterings in the first three rows result in very similar filtered bundles, each one differing only slightly from the others. Interestingly, the spatial pruning method (fourth row) displays a qualitatively different behaviour with respect to track elimination. Most prominent is the fact that the fanning of the bundle is gradually destroyed (which is to be expected by the fourth method's operational construction enforcing coherence in the spatial domain), whereas this is retained by using tractometric filtering (which cannot be expected a priori).

In the second experiment, on the clinical dataset, we consider the AF bundle, cf. Fig. 4. At first glance there appears to be a number of shortcuts in the tractograms. This behaviour is reflected in the scatterplots, revealing two point clusters. In all cases, tractometric filtering removes first the smaller cluster, thereby eliminating the shortcuts from the tractogram, in correspondence with spatial FBC-based pruning. In this case, spatial coherence of tracks apparently correlates strongly with intrinsic tractometric features.

4 Discussion

We have proposed a method for filtering diffusion MRI tractograms. Based on the assumption that anatomical (sub)bundles are internally structurally coherent, we have constructed characteristic trackwise scalar invariants, combined into complete and non-redundant sets so as to capture all degrees of freedom of a given differential order. For each track, the associated set of invariants defines coordinates of a point in a feature space. The tractogram of the bundle of interest is then effectively filtered by removing outliers from the corresponding point cloud in this space.

Experiments indicate that this method may be used in conjunction to existing methods, such as filters based on spatial coherence of the tracks. It depends on the anatomical bundle of interest which method is most appropriate. Whereas spatial filters will tend to eliminate spatial outliers by construction, tractometric filters are blind to spatial configurations and driven by intrinsic characteristics of individual tracks. For instance, sub-bundles or branches of a fanning bundle may or may not have distinct intrinsic characteristics. Future research should

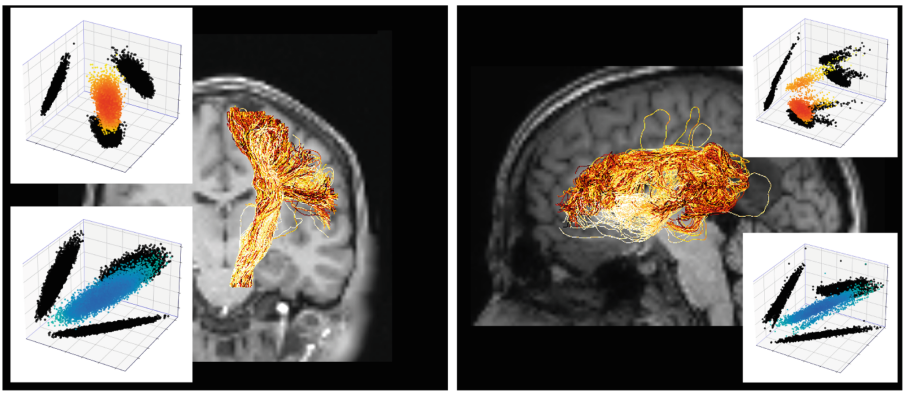

Fig. 2. The baseline tractograms for experiments on the CST (left) and AF (right). The former experiment is performed on the HCP dataset and the latter on the clinical dataset. The scatterplots depict the diffusion invariants (red-yellow) and the curvature invariants (light-dark blue). The tractograms are color-coded according to the isolation score ranking corresponding to the diffusion invariants. While we could have chosen to use the curvature invariants or the union of both sets, this is merely a practical choice to illustrate the behaviour of scalar features in the tractogram. (Color figure online)

help to identify the 'elementary' anatomical (sub-)bundles for which a particular method is appropriate. A clustering method applied prior to pruning in the case of multi-modal point clouds might be instrumental. Experiments with multiple (sub-)bundles in the same subject as well as studying the inter-subject variability of this method are interesting avenues for further research.

Interestingly, by employing distinct sets of independent invariants, viz. diffusion and curvature invariants, one may a priori expect a difference in the outcome. However, the experiments show that, at least qualitatively, using each in isolation or combining both, hardly affects the result. This is an indication that the premise of microstructural coherence of an anatomically plausible bundle might be correct, since that would reflect itself in macroscopic coherence of invariants regardless of their precise nature.

Our framework can be extended in multiple ways. One may add new sets of invariants and consider various combinations. Considering higher order derivatives of the metric tensor field can systematically add complexity to the sets of invariants. Moreover, extrinsic spatial (such as FBC) and intrinsic tractometric features may be combined in a hybrid method. Other integral or projective operators to construct invariant functionals, besides the simple case of the mean operator used in this paper, may be considered. In particular one may define point-wise invariant functionals for each tract, leading to more complex, high-dimensional descriptors of a tractogram. Our framework may find applicability beyond DTI, e.g. using RISH features for the spherical harmonic representation of fiber orientation density functions [24].

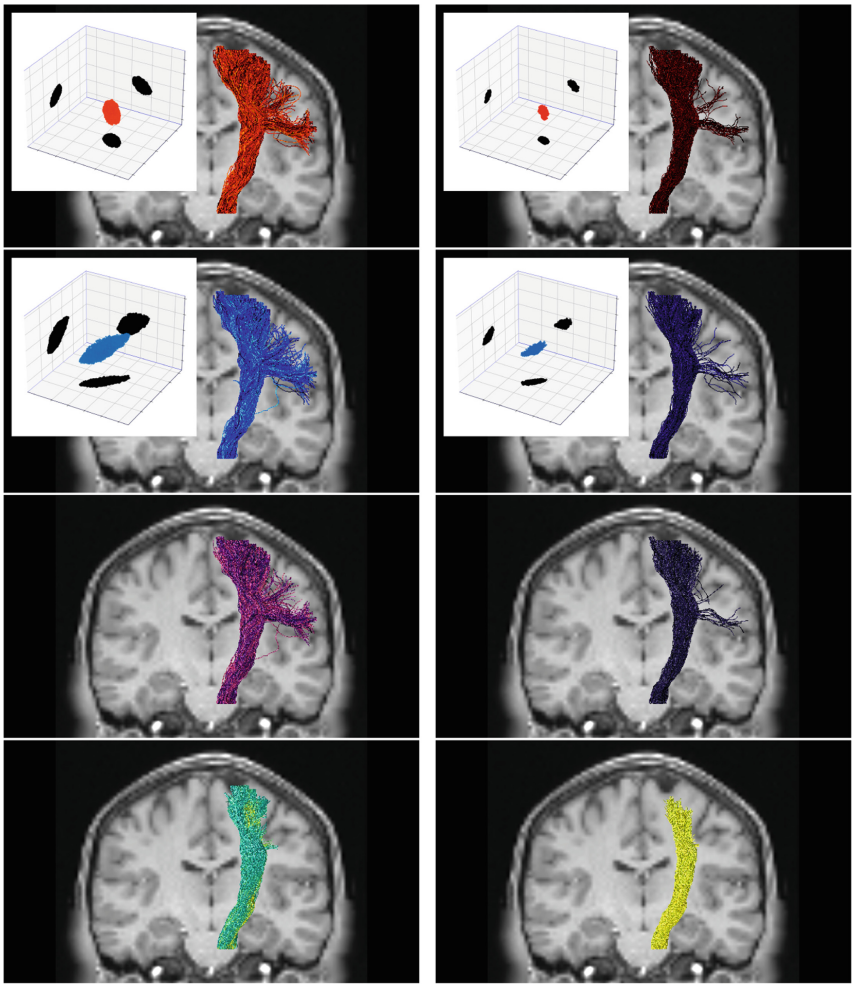

Fig. 3. The effect of filtering the CST tractograms, see Fig. 2, with different sets of invariants as well as using a spatial filter. Each row represents a different filter and each column a threshold by which to prune the tractogram (expressed in percentage of the total number of tracks). **Columns:** Filtered tractograms with 50%, resp. 10% of the tracks remaining. **Rows 1–4:** Diffusion invariants and corresponding scatterplot; Curvature invariants and corresponding scatterplot; Combined diffusion and curvature invariants; Fiber-to-Bundle Coherence.

Secondly, even though tractometry is only applied to streamline tractograms in our experiments, the curvature invariants would have a more transparent interpretation in a Riemannian geodesic framework, for which they were designed in the first place in the context of uncertainty quantification given data perturbations (noise and end-point conditions). Interpretability of features in terms of

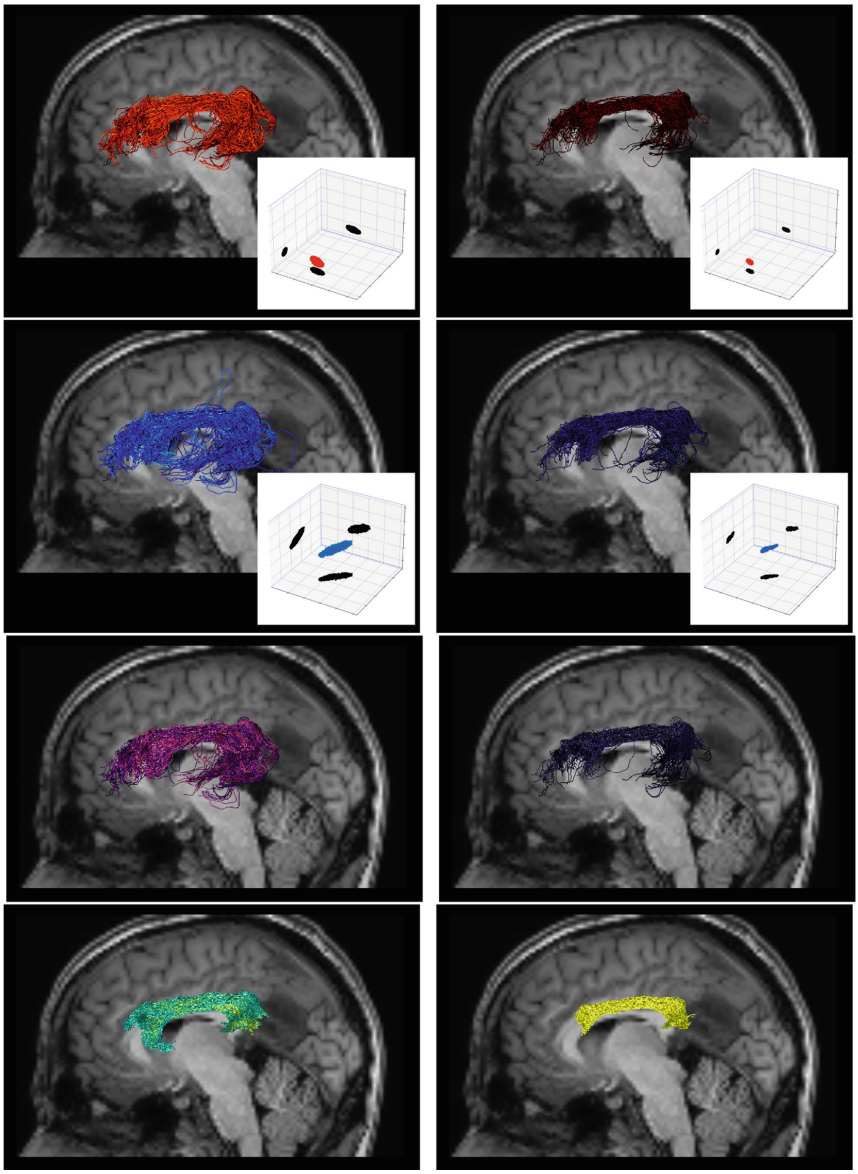

Fig. 4. The effect of filtering the AF tractograms with different sets of invariants as well as using a spatial filter. Each row represents a different filter and each column a threshold by which to prune the tractogram (expressed in percentage of the total number of tracks). Filtered tractograms with 50%, resp. 10% of the tracks remaining. **Rows 1–4:** Diffusion invariants and corresponding scatterplot; Curvature invariants and corresponding scatterplot; Combined diffusion and curvature invariants; Fiber-to-Bundle Coherence.

the specific details of a tractography method is, however, subordinate to completeness. Complete sets of tractometric invariants can therefore be applied to prune any tractogram, regardless of its operational definition.

Acknowledgements. This work is part of the research programme "Diffusion MRI Tractography with Uncertainty Propagation for the Neurosurgical Workflow" with project number 16338, which is (partly) financed by the Netherlands Organisation for Scientific Research (NWO). This work was supported by a research grant (00028384) from VILLUM FONDEN. We would like to thank neurosurgeon Geert-Jan Rutten for sharing the clinical dataset used in our experiments at the Elisabeth TweeSteden Hospital (ETZ) in Tilburg, The Netherlands, and for fruitful discussions.

References

1. Bao, D., Chern, S.S., Shen, Z.: An Introduction to Riemann-Finsler Geometry. Graduate Texts in Mathematics, vol. 2000. Springer, New York (2000). https://doi.org/10.1007/978-1-4612-1268-3
2. Basser, P.J., Pajevic, S., Pierpaoli, C., Duda, J., Aldroubi, A.: In vivo fiber tractography using DT-MRI data. Magn. Reson. Med. **44**(4), 625–632 (2000)
3. Basser, P.J., Pierpaoli, C.: Microstructural and physiological features of tissues elucidated by quantitative-diffusion-tensor MRI. J. Magn. Reson. Series B **111**(3), 209–219 (1996)
4. Behrens, T.E.J., Berg, H.J., Jbabdi, S., Rushworth, M.F.S., Woolrich, M.W.: Probabilistic diffusion tractography with multiple fibre orientations: what can we gain? Neuroimage **34**(1), 144–155 (2007)
5. Breunig, M.M., Kriegel, H.P., Ng, R.T., Sander, J.: LOF: identifying density-based local outliers. In: Proceedings of the 2000 ACM SIGMOD International Conference on Management of Data, pp. 93–104. SIGMOD 2000, Association for Computing Machinery, New York, NY, USA (2000)
6. Chamberland, M., et al.: Tractometry-based anomaly detection for single-subject white matter analysis (2020)
7. Chamberland, M., et al.: Dimensionality reduction of diffusion MRI measures for improved tractometry of the human brain. Neuroimage **200**, 89–100 (2019)
8. Coley, A.A., MacDougall, A., McNutt, D.D.: Basis for scalar curvature invariants in three dimensions. Class. Quantum Gravity **31**(23), 235010 (2014)
9. Coley, A., Hervik, S., Pelavas, N.: Spacetimes characterized by their scalar curvature invariants. Class. Quantum Gravity **26**(2), 025013 (2009)
10. Daducci, A., Dal Palù, A., Lemkaddem, A., Thiran, J.P.: Commit: convex optimization modeling for microstructure informed tractography. IEEE Trans. Med. Imaging **34**(1), 246–257 (2015)
11. Fuster, A., Dela Haije, T., Tristán-Vega, A., Plantinga, B., Westin, C.F., Florack, L.: Adjugate diffusion tensors for geodesic tractography in white matter. J. Math. Imaging Vis. **54**(1), 1–14 (2016)
12. Garyfallidis, E., et al.: Dipy, a library for the analysis of diffusion MRI data. Front. Neuroinf. 8 (2014)
13. Garyfallidis, E., Brett, M., Correia, M.M., Williams, G.B., Nimmo-Smith, I.: QuickBundles, a method for tractography simplification. Front. Neurosci. **6**, 175 (2012)

14. Garyfallidis, E., et al.: Recognition of white matter bundles using local and global streamline-based registration and clustering. Neuroimage **170**, 283–295 (2018)
15. Hao, X., Whitaker, R.T., Fletcher, P.T.: Adaptive Riemannian metrics for improved geodesic tracking of white matter. In: Székely, G., Hahn, H.K. (eds.) IPMI 2011. LNCS, vol. 6801, pp. 13–24. Springer, Heidelberg (2011). https://doi.org/10.1007/978-3-642-22092-0_2
16. Hao, X., Zygmunt, K., Whitaker, R.T., Fletcher, P.T.: Improved segmentation of white matter tracts with adaptive Riemannian metrics. Med. Image Anal. **18**, 161–175 (2014)
17. Jost, J.: Riemannian Geometry and Geometric Analysis. Universitext, 6th edn. Springer, Berlin (2011). https://doi.org/10.1007/978-3-642-21298-7
18. Knorr, E.M., Ng, R.T., Tucakov, V.: Distance-based outliers: algorithms and applications. VLDB J. **8**(3), 237–253 (2000)
19. Legarreta, J.H., et al.: Filtering in tractography using autoencoders (FINTA). Med. Image Anal. **72**, 102126 (2021)
20. Lenglet, C., Deriche, R., Faugeras, O.: Inferring white matter geometry from diffusion tensor MRI: application to connectivity mapping. In: Pajdla, T., Matas, J. (eds.) ECCV 2004. LNCS, vol. 3024, pp. 127–140. Springer, Heidelberg (2004). https://doi.org/10.1007/978-3-540-24673-2_11
21. Liu, F.T., Ting, K.M., Zhou, Z.H.: Isolation forest. In: 2008 Eighth IEEE International Conference on Data Mining, pp. 413–422 (2008)
22. Meesters, S., et al.: Stability metrics for optic radiation tractography: towards damage prediction after resective surgery. J. Neurosci. Methods **288**, 34–44 (2017)
23. Meesters, S., Rutten, G.J., Fuster, A., Florack, L.: Automated tractography of four white matter fascicles in support of brain tumor surgery. In: 2019 OHBM Annual Meeting, June 6–13 2019, Rome, Italy. Organization for Human Brain Mapping (2019), abstract nr. Th768
24. Mirzaalian, H., et al.: Harmonizing diffusion MRI data across multiple sites and scanners. In: Medical image computing and computer-assisted intervention: MICCAI ... International Conference on Medical Image Computing and Computer-Assisted Intervention 9349, 12–19 October (2015)
25. O'Donnell, L., Haker, S., Westin, C.-F.: New approaches to estimation of white matter connectivity in diffusion tensor MRI: Elliptic PDEs and geodesics in a tensor-warped space. In: Dohi, T., Kikinis, R. (eds.) MICCAI 2002. LNCS, vol. 2488, pp. 459–466. Springer, Heidelberg (2002). https://doi.org/10.1007/3-540-45786-0_57
26. O'Donnell, L., Westin, C.F.: Automatic tractography segmentation using a high-dimensional white matter atlas. IEEE Trans. Med. Imaging **26**, 1562–75 (2007)
27. Rund, H.: The Differential Geometry of Finsler Spaces. Springer, Berlin (1959). https://doi.org/10.1007/978-3-642-51610-8
28. Schober, M., Kasenburg, N., Feragen, A., Hennig, P., Hauberg, S.: Probabilistic shortest path tractography in DTI Using Gaussian process ODE solvers. In: Golland, P., Hata, N., Barillot, C., Hornegger, J., Howe, R. (eds.) MICCAI 2014. LNCS, vol. 8675, pp. 265–272. Springer, Cham (2014). https://doi.org/10.1007/978-3-319-10443-0_34
29. Sebastiani, G., De Pasquale, F., Barone, P.: Quantifying human brain connectivity from diffusion tensor MRI. J. Math. Imaging is. **25**(2), 227–244 (2006)
30. Sengers, R., Florack, L., Fuster, A.: Geodesic uncertainty in diffusion MRI. Front. Comput. Sci. **3**, 718131 (2021)

31. Sengers, R., Florack, L., Fuster, A.: Geodesic tubes for uncertainty quantification in diffusion MRI. In: Feragen, A., Sommer, S., Schnabel, J., Nielsen, M. (eds.) IPMI 2021. LNCS, vol. 12729, pp. 279–290. Springer, Cham (2021). https://doi.org/10.1007/978-3-030-78191-0_22
32. Shen, Y.B., Shen, Z.: Introduction to Modern Finsler Geometry. World Scientific, Singapore (2016)
33. Smith, R.E., Tournier, J.D., Calamante, F., Connelly, A.: Sift2: enabling dense quantitative assessment of brain white matter connectivity using streamlines tractography. Neuroimage **119**, 338–351 (2015)
34. Spivak, M.: Differential Geometry, vol. 1–5. Publish or Perish, Berkeley (1975)
35. St-Jean, S., Chamberland, M., Viergever, M.A., Leemans, A.: Reducing variability in along-tract analysis with diffusion profile realignment. Neuroimage **199**, 663–679 (2019)
36. Tournier, J.D., Smith, R., Raffelt, D., Tabbara, R., Dhollander, T., Pietsch, M., Christiaens, D., Jeurissen, B., Yeh, C.H., Connelly, A.: MRtrix3: a fast, flexible and open software framework for medical image processing and visualisation. Neuroimage **202**, 116137 (2019)
37. Westin, C.-F., Maier, S.E., Khidhir, B., Everett, P., Jolesz, F.A., Kikinis, R.: Image processing for diffusion tensor magnetic resonance imaging. In: Taylor, C., Colchester, A. (eds.) MICCAI 1999. LNCS, vol. 1679, pp. 441–452. Springer, Heidelberg (1999). https://doi.org/10.1007/10704282_48
38. Yeatman, J.D., Dougherty, R.F., Myall, N.J., Wandell, B.A., Feldman, H.M.: Tract profiles of white matter properties: automating fiber-tract quantification. PLoS ONE **7**(11), e49790 (2012)